

Three-dimensional endoscopic optical coherence tomography by use of a two-axis microelectromechanical scanning mirror

Woonggyu Jung^{a)}

Beckman Laser Institute, University of California, Irvine, California 92617
and Department of Biomedical Engineering, University of California, Irvine, California 92617

Daniel T. McCormick

Department of Electrical Engineering and Computer Science, University of California, Berkeley, California 94720 and Berkeley Sensor and Actuator Center and Adriatic Research Institute, Berkeley, California 94720

Jun Zhang and Lei Wang

Beckman Laser Institute, University of California, Irvine, California 92617

Norman C. Tien

Department of Electrical Engineering and Computer Science, Case Western Reserve University, Cleveland, Ohio 44106

Zhongping Chen^{b)}

Beckman Laser Institute, University of California, Irvine, California 92617
and Department of Biomedical Engineering, University of California, Irvine, California 92617

(Received 10 November 2005; accepted 15 March 2006; published online 17 April 2006)

We present a three-dimensional (3D) endoscopic optical coherence tomography (OCT) system based on a dual-axis scanning microelectromechanical system (MEMS) mirror. The diameter of the MEMS mirror was 1.2 mm and both axes were capable of scanning greater than 20° with linearity. The endoscopic MEMS probe was integrated with an OCT system and volume images were obtained at a rate of 3 frames/s by means of two-axis lateral scanning combined with an axial scan. In the initial investigations, 3D OCT images of healthy rabbit trachea as well as images of normal and cancerous regions of hamster cheek pouch tissue were obtained. © 2006 American Institute of Physics. [DOI: 10.1063/1.2195092]

Optical coherence tomography (OCT) is an emerging technology that is capable of high resolution, minimally invasive, nondestructive, and real time imaging.^{1,2} OCT is based on optical coherence reflectometry which is analogous to ultrasound imaging but utilizes a broadband light source instead of sound waves to measure the intensity of back reflection as function of depth in the sample. OCT has been used effectively for cross-sectional imaging in the fields of medicine and biophotonics.²⁻⁵ In order to provide access to the internal organs, various miniaturized OCT probes that provide either linear or rotational scanning have been developed.^{2,5-7} However, conventional endoscopic OCT probes suffer from low scanning speed, nonuniform coupling, and are limited to one-dimensional (1D) scanning. The recent development of Fourier-domain OCT (FD-OCT) has significantly increased the imaging speed achievable by OCT systems.^{8,9} High speed two-dimensional (2D) as well as three-dimensional (3D) OCT imagings require scanning probes with performance parameters that cannot be achieved with conventional OCT probes. Therefore, advanced endoscopic probes that provide high speed, reliable 2D scanning at a low cost are essential.

In this letter, we report a three-dimensional endoscopic OCT system employing a two-axis microelectromechanical scanning mirror to achieve 3D imaging. Microelectromechanical system (MEMS) is an enabling technology allowing the integration of mechanical elements, sensors, actuators,

and electronics on a common substrate, such as silicon, via the use of microfabrication technologies. MEMS technologies offer many advantages, including low power consumption, small size, precise feature control, and high operation speeds; therefore, they have received a great deal of attention for a wide range of applications. Pan *et al.* and Zara *et al.* have utilized a MEMS device to demonstrate 1D scanning for endoscopic OCT.^{10,11} However, a 1D scanning mirror is only capable of providing a 2D image. In many cases, 2D imaging provides insufficient information to fully identify and visualize morphological features or to determine the margins of diseased tissue in clinic applications. Therefore, we introduce a 3D endoscopic probe employing a 2D scanning MEMS mirror and demonstrate preliminary results to evaluate its performance.

Figure 1(a) presents a scanning electron microscope (SEM) image of a two-axis MEMS mirror. The MEMS scanning actuator employed in this work is monolithic, single crystal silicon (SCS), two-dimensional, gimbal-less, vertical comb-driven structure employing electrostatic forces for actuation.^{12,13} As the devices are fabricated from SCS, there is no intrinsic stress or drift of mechanical properties, such as Young's modulus, under normal operating conditions. Furthermore, there are no known failure modes provided that the ultimate strain levels of the silicon are not exceeded. In addition, due to the use of vertical comb-drive electrostatic actuators, the device does not have any contacting or rubbing surfaces. As a result, the devices exhibit excellent long term reliability and precision. The devices are designed and realized in a self-aligned deep reactive ion etching (DRIE) fab-

^{a)}Electronic mail: jungw@uci.edu

^{b)}Electronic mail: z2chen@uci.edu

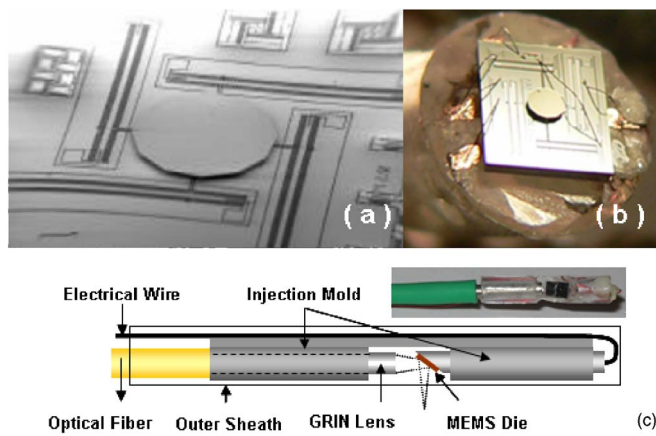


FIG. 1. (Color online) (a) A scanning electron microscope (SEM) image of a two-axis MEMS mirror. (b) An optical micrograph of a scanner with attached mirror with wire bond connections to an acrylic package. (c) Schematic and photograph of completed 3D endoscopic MEMS probe ($D_{\text{outer}} < 4$ mm). The photograph of the probe was taken without outer sheath.

rication process utilizing a silicon on insulator (SOI) wafer. The mirrors are fabricated in a separate SOI process and later bonded to the actuator, allowing the actuator and mirror to be independently optimized. The mirror apertures are metalized low-inertia SCS structures consisting of a thinned mirror plate (2–5 μm), thick stiffening trusses (~ 25 μm), and a tall standoff pedestal (~ 120 μm). The device employed in this particular study has a 1.2 mm diameter mirror and exhibited x - and y -axis resonant frequencies of 1.8 and 2.4 kHz, respectively. The scan angle of each axis is 20° (optical). The maximum static drive voltage applied to the mirror in this experiment was 100 V, and the device is driven such that a linear scan with constant velocity is achieved. During characterization of the probe, the accuracy as well as precision of the scan were verified employing a position sensitive diode (PSD) and optical feedback system. The characterization system was also employed to obtain the optimized scan pattern for a specific application of the OCT system. The characterization system generates custom drive wave forms and filters based on the measured angle versus voltage characteristic tables and small-signal second order system frequency response characteristics of individual devices. The amplifier driving the devices delivered a maximum voltage of 150 V during drive transients; however, the electrostatic comb structures require very small current levels to operate and the amplifier incorporates several protection mechanisms. The devices were packaged in a custom machined acrylic package, which provides mechanical rigidity and protection as well as the electrical connections for the MEMS device. The MEMS scanners were diced during the fabrication process, eliminating the possibility of damage and contamination from a scribing or wafer sawing step. The endoscopic package was realized from a single extruded acrylic rod with an outer diameter of < 4 mm; concentric holes sharing the same center point were drilled along the central axis, following a common guide hole, in order to allow accurate and precise alignment of the optical components. Six small (300 μm in diameter) holes were then drilled from the distal end of the probe in order to provide electrical connections to the mirror. A 45° platform was then machined to serve as a support for the mirror die; sufficient material remained on the tube walls to maintain mechanical

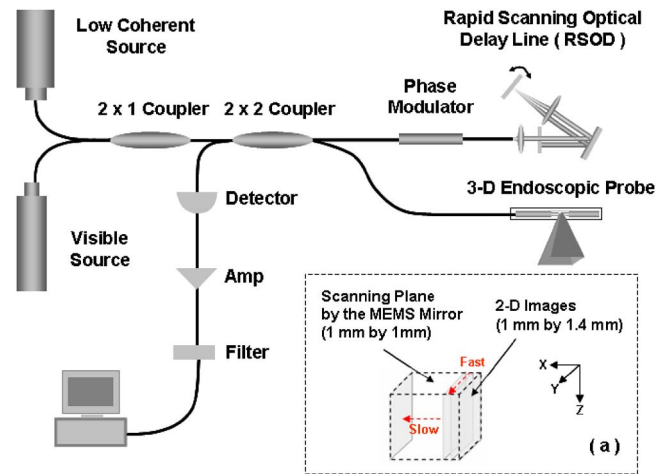


FIG. 2. (Color online) Schematic of 3D endoscopic OCT system. (a) shows scanning methodology of the MEMS mirror and the generation of a volume image by stacking of images. X and Y axes indicate slow and fast axis scanning by MEMS mirror and Z axis presents depth scanning by RSOD.

rigidity and structural integrity [Fig. 1(b)]. Wires with a diameter of 200 μm were then passed through the access holes and secured in place with epoxy; the surface of the wires were then planarized and served as bonding pads. The tail of the wires was bent back and run through a channel along the bottom of the probe. A graded index (GRIN) lens with a pigtailed optical fiber was inserted into the package and temporarily held in place while the MEMS mirror was positioned on the machined platform. The course alignment of the components utilized a stereoscope and a visible laser coupled into the GRIN lens. The mirror was then fixed in place and the wire bond connections were made between the MEMS die and the package. With the visible and 1310 nm source, alignment and operation were verified; after the desired focal point location was achieved, the GRIN lens was then permanently fixed in the package. The specific GRIN lens ($\phi 1.4$ mm) utilized in this study had a 6.6 mm working distance and approximately 20 μm spot size at the focal plane. A schematic and photograph of the packaged endoscopic OCT probe with MEMS mirror is presented in Fig. 1(c).

The packaged endoscopic probe was integrated with a fiber-based OCT system as shown in Fig. 2. The system employed a low-coherence-length light source that delivered an output power of 10 mW at a central wavelength of 1310 nm with a bandwidth of 80 nm, providing 10 μm axial resolution. A visible aiming beam (633 nm) was utilized to locate the exact position and path on the sample, and both light sources were coupled into a fiber-based Michelson interferometer. In the reference arm, a rapid-scanning optical delay line (RSOD) was used that employed a grating to control the phase and group delays separately so that no phase modulation was introduced when the group delay was scanned.¹⁴ The phase modulation was generated through an electro-optic phase modulator that produced a stable carrier frequency. The axial line scanning rate was 500 Hz, and the modulation frequency was 500 kHz. In the sampling arm, the previously described MEMS scanner was employed to provide sample scanning; the MEMS device was controlled by custom electronics interfaced to the OCT data acquisition system. 2D cross-sectional image is acquired by lateral scan (A scan) by one-axis scanning of the MEMS scanner and

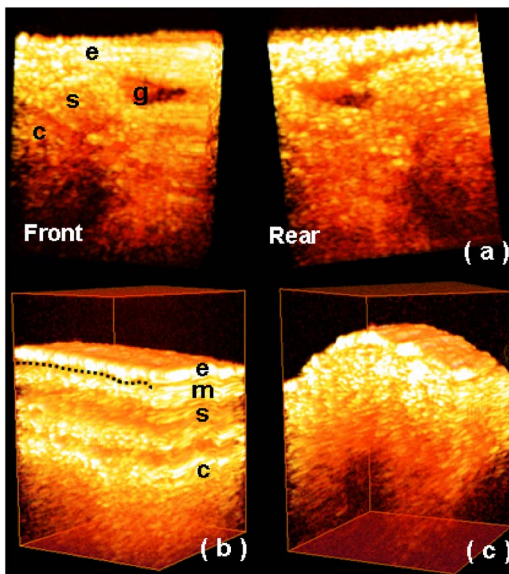


FIG. 3. (Color online) 3D OCT images obtained by endoscopic OCT system using the dual-axis scanning MEMS probe. (a) Image of rabbit trachea at front and rear. Important tracheal structures such as the epithelium (e), glands (g), submucosa (s), and cartilage (c) are clearly visible. (b) Image of normal hamster cheek pouch. Vivid layered structures including the epithelium (e), and mucosa (m), submucosa (s) are visualized. (c) At the bottom of the image, the cork plate which was used to hold tissue is visible. The dotted line indicates the base membrane. (c) OCT image of cancerous hamster cheek pouch tissue.

depth scan (B scan) by RSOD. In an analogous manner with 2D imaging, for 3D OCT imaging, a 2D image is first achieved by the combination of one-axis scanning of the MEMS scanner sequentially after each depth scanning of the RSOD. Then, the second axis of the MEMS mirror moves one “step” to the next position and another 2D image is obtained. This routine is continuously repeated until the scanning area specified by the operator is completed. In Fig. 2, the dashed box provides a schematic summary of the 3D scanning methodology. The reflected beams from the sample and reference arms were recombined in the interferometer and the detected optical interference fringes signals from the photodetector were filtered at the carrier frequency. The resulting signals were automatically displayed as 2D images in real time, saved on the computer, accumulated, and visualized as a 3D image after postimage processing, such as isosurface extraction, filtering, thresholding, pseudocoloring, animation, and region selection.

Figure 3 presents 3D images acquired by the 3D MEMS based endoscopic OCT system. As previously noted, volume images were obtained at a rate of 3 frames/s via two-axis lateral scanning combined with an axial scan. The images obtained in this work were $1 \times 1 \times 1.4 \text{ mm}^3$ ($400 \times 200 \times 560$ pixels). In the 3D images, thresholding is used to remove background, such as air, and we visualize only biological tissue structures of interest. Figure 3(a) presents a 3D image of a section of rabbit trachea at 180° camera perspectives. In both images, tissue structures, such as the epithelium, submucosa, glands, and cartilage, were clearly visualized. To further evaluate the feasibility of the 3D MEMS probe for clinic application, both normal and cancerous regions of tissue from a hamster cheek pouch were imaged (shown in Figs. 3(b) and 3(c)). In the OCT image of normal tissue, Fig. 3(b), the layered structures (e.g., epithe-

lium, mucosa, and submucosa) are clearly visible with vivid border lines, including the basement membrane. This membrane provides basic information regarding identification and diagnosis of precancer, such as dysplasia. In contrast to the image of normal tissue, layered structures are not visible and the base membrane is not distinguished clearly in the cancerous tissue as presented in Fig. 3(c). This result demonstrated that 3D endoscopic OCT is a promising tool to visualize useful morphology at any location using post-image processing.

In summary, we have realized a 3D endoscopic OCT system employing a two-axis MEMS scanning probe and have demonstrated its potential as a real-time tool for optical biopsy. A MEMS mirror actuated by electrostatic comb drives was incorporated with a pigtailed GRIN lens and packaged. The final 3D endoscopic probe has an outer diameter of $<4 \text{ mm}$ and was integrated with a fiber-based OCT system. Biological tissues from a rabbit and a hamster were imaged; the resulting volume images provided morphological details such as visualization of the epithelium, mucosa, and submucosa. In particular, the basement membrane line was readily identified in 3D images from normal hamster cheek pouch tissue; in regions of cancerous growth, the lack of an identifiable basement membrane was clearly distinguished in real time. In the presented work, the frame rate was not determined by the MEMS scanner; it was limited by the speed of the RSOD line and configuration of the sampling hardware. In further studies, faster image speed could be achieved if a high speed system, such as the FD-OCT, is incorporated with our MEMS scanner.

The authors acknowledge the contribution of V. Milanović with D. McCormick at the Adriatic Research Institute for mirror fabrication and wire bonding. This work was supported by research grants from the National Science Foundation (BES-86924), National Institutes of Health (EB-00255, NCI-91717, and RR-01192), and the Air Force Office of Scientific Research (FA9550-04-1-0101). Institutional support from the Beckman Laser Institute Endowment is also gratefully acknowledged.

- ¹D. Huang, E. A. Swanson, C. P. Lin, J. S. Schuman, W. G. Stinson, W. Chang, M. R. Hee, T. Flotte, K. Gregory, C. A. Puliafito, and J. G. Fujimoto, *Science* **254**, 1178 (1991).
- ²G. J. Tearney, M. E. Brenzinski, B. E. Bouma, S. A. Boppart, C. Pitris, J. F. Southern, and J. G. Fujimoto, *Science* **276**, 2037 (1997).
- ³M. R. Hee, J. A. Izatt, E. A. Swanson, D. Huang, C. P. Lin, J. S. Schuman, C. A. Puliafito, and J. G. Fujimoto, *Arch. Ophthalmol. (Chicago)* **113**, 326 (1995).
- ⁴L. Wang, W. Xu, M. Backman, G. P. Li, and Z. Chen, *Appl. Phys. Lett.* **85**, 1855 (2004).
- ⁵A. M. Rollins, R. Ung-arunyawee, A. Chak, R. C. K. Wong, K. Kobayashi, M. V. Sivak, and J. A. Izatt, *Opt. Lett.* **24**, 1358 (1999).
- ⁶B. E. Bouma and G. J. Tearney, *Opt. Lett.* **24**, 531 (1999).
- ⁷Y. Wang, M. Bachman, G. P. Li, S. Guo, B. J. F. Wong, and Z. Chen, *Opt. Lett.* **30**, 53 (2005).
- ⁸J. Zhang, J. S. Nelson, and Z. Chen, *Opt. Lett.* **30**, 147 (2005).
- ⁹S. H. Yun, G. J. Tearney, J. F. de Boer, N. Iftimia, and B. E. Bouma, *Opt. Express* **11**, 2953 (2003).
- ¹⁰Y. Pan, H. Xie, and G. K. Fedder, *Opt. Lett.* **26**, 1966 (2001).
- ¹¹J. M. Zara, S. Yazdanfar, K. D. Rao, J. A. Izatt, and S. W. Smith, *Opt. Lett.* **28**, 628 (2003).
- ¹²V. Milanović, *J. Microelectromech. Syst.* **13**, 19 (2004).
- ¹³V. Milanović, D. T. McCormick, and G. Matus, *IEEE J. Sel. Top. Quantum Electron.* **10**, 462 (2004).
- ¹⁴G. J. Tearney, B. E. Bouma, and F. G. Fujimoto, *Opt. Lett.* **22**, 1811 (1997).